Journal of Cerebral Blood Flow & Metabolism (2014) 34, 1188–1196

www.jcbfm.com

ORIGINAL ARTICLE

Serotonin 2A receptor agonist binding in the human brain with [^{11}C]Cimbi-36

Anders Ettrup[1], Sophie da Cunha-Bang[1], Brenda McMahon[1], Szabolcs Lehel[2], Agnete Dyssegaard[1], Anine W Skibsted[1], Louise M Jørgensen[1], Martin Hansen[3], Anders O Baandrup[4], Søren Bache[5], Claus Svarer[1], Jesper L Kristensen[3], Nic Gillings[2], Jacob Madsen[2] and Gitte M Knudsen[1]

[^{11}C]Cimbi-36 was recently developed as a selective serotonin 2A (5-HT$_{2A}$) receptor agonist radioligand for positron emission tomography (PET) brain imaging. Such an agonist PET radioligand may provide a novel, and more functional, measure of the serotonergic system and agonist binding is more likely than antagonist binding to reflect 5-HT levels *in vivo*. Here, we show data from a first-in-human clinical trial with [^{11}C]Cimbi-36. In 29 healthy volunteers, we found high brain uptake and distribution according to 5-HT$_{2A}$ receptors with [^{11}C]Cimbi-36 PET. The two-tissue compartment model using arterial input measurements provided the most optimal quantification of cerebral [^{11}C]Cimbi-36 binding. Reference tissue modeling was feasible as it induced a negative but predictable bias in [^{11}C]Cimbi-36 PET outcome measures. In five subjects, pretreatment with the 5-HT$_{2A}$ receptor antagonist ketanserin before a second PET scan significantly decreased [^{11}C]Cimbi-36 binding in all cortical regions with no effects in cerebellum. These results confirm that [^{11}C]Cimbi-36 binding is selective for 5-HT$_{2A}$ receptors in the cerebral cortex and that cerebellum is an appropriate reference tissue for quantification of 5-HT$_{2A}$ receptors in the human brain. Thus, we here describe [^{11}C]Cimbi-36 as the first agonist PET radioligand to successfully image and quantify 5-HT$_{2A}$ receptors in the human brain.

Journal of Cerebral Blood Flow & Metabolism (2014) **34,** 1188–1196; doi:10.1038/jcbfm.2014.68; published online 30 April 2014

Keywords: agonist; clinical; kinetic modeling; positron emission tomography; 5-HT$_{2A}$ receptor

INTRODUCTION

The neurotransmitter serotonin (5-HT) is a modulator of a vast variety of normal physiologic effects and is also involved in the pathophysiology of central nervous system disorders such as depression and schizophrenia. The serotonin 2A (5-HT$_{2A}$) receptor is the main excitatory 5-HT receptor in the human central nervous system, it is responsible for the hallucinogenic effects of recreational agonist drugs such as lysergic acid diethylamide and psilocybin, and 5-HT$_{2A}$ receptor antagonism is a characteristic of atypical antipsychotics.[1] Furthermore, changes in 5-HT$_{2A}$ receptor levels have been linked to the pathophysiology of human diseases such as depression.[2,3]

Positron emission tomography (PET) has unsurpassed sensitivity and selectivity to detect and quantify specific proteins and processes in the human brain. Positron emission tomography imaging with radioligands is a widely used tool to quantify differences in receptor binding, for example, between patient and control groups, to quantify receptor occupancy of pharmacological interventions or to measure neurotransmitter release *in vivo*.[4,5]

In clinical studies, 5-HT$_{2A}$ receptor antagonists have for decades been in use as PET radioligands, most notably [^{18}F]altanserin and [^{11}C]MDL100907.[6] However, agonist PET radioligands may functionally possess several advantages over antagonists. Importantly, agonist radioligands in the dopamine system have an increased sensitivity to endogenously released neurotransmitter. Here, several studies using pharmacologically increased dopamine levels find larger decreases in the receptor binding of agonist as compared with antagonist PET radioligands.[5,7] This increased sensitivity of agonist radioligands in comparison with antagonists has been hypothesized to be due to the agonists binding the high-affinity state of the receptors selectively while the antagonists bind the total pool of receptor with equal affinity. This supports the notion that agonists bind active receptors selectively *in vivo* and agonist binding should thus serve as a more accurate functional measure of receptor binding. The existence of two affinity states is well-established *in vitro* but whether agonist PET radioligands bind high-affinity state of receptors *in vivo* is still subject to debate.[5] The sensitivity of agonist PET radioligands to endogenously released neurotransmitter is interesting for targets in the 5-HT system as such a ligand may be inversely correlated with acute changes in 5-HT levels in the living brain. Thus, PET radioligand binding may serve as a biomarker for the function of the serotonergic system which, in turn, could prove a highly disease-relevant measure. This is the first 5-HT$_{2A}$ receptor agonist radioligand to be validated for applications in the human brain. Also, the 5-HT$_{2A}$ receptor antagonist PET radioligands available for human use have displayed limited or no sensitivity to endogenously released 5-HT,[8–10] further underlining the potential for an agonist radioligand for this target in humans.

[^{11}C]Cimbi-36 was developed as an agonist radioligand for brain imaging of 5-HT$_{2A}$ receptors with PET in the pig brain.[11]

[1]Neurobiology Research Unit and Center for Integrated Molecular Brain Imaging (CIMBI), Copenhagen University Hospital, Rigshospitalet, Copenhagen, Denmark; [2]PET- and Cyclotron Unit, Copenhagen University Hospital, Rigshospitalet, Copenhagen, Denmark; [3]Department of Drug Design and Pharmacology, Faculty of Health and Medical Sciences, University of Copenhagen, Copenhagen, Denmark; [4]Department of Radiology, Copenhagen University Hospital, Rigshospitalet, Copenhagen, Denmark and [5]Department of Neuroanaesthesiology, Copenhagen University Hospital, Rigshospitalet, Copenhagen, Denmark. Correspondence: Dr A Ettrup or Professor GM Knudsen, Neurobiology Research Unit, Copenhagen University Hospital, Rigshospitalet, Building 6931, Blegdamsvej 9, 2100 Copenhagen, Denmark.
E-mail: ettrup@nru.dk or gmk@nru.dk
This study was financially supported by the Lundbeck Foundation, the Arvid Nilssons Foundation, the Toyota Foundation, and the John and Birthe Meyer Foundation.
Received 13 February 2014; revised 26 March 2014; accepted 27 March 2014; published online 30 April 2014

Here, Cimbi-36 was found to be highly selective for 5-HT_{2A} and 5-HT_{2C} receptors over >40 other neuroreceptor targets tested, and Cimbi-36 was found a full agonist at 5-HT_{2A} receptors. We further showed its *in vivo* agonistic effects in mice and showed reasonable radiation dosimetry associated with PET imaging with [^{11}C]Cimbi-36.[12] Furthermore, that Cimbi-36 in pharmacological doses acts as 5-HT_{2A} receptor agonist in humans is attested by its problematic misuse as a recreational hallucinogenic drug (aliases include 25B or 25B-NBOMe[13]), which has also led to placement of the compound in the Drug Enforcement Administration's schedule one of the Controlled Substances Act.[14] In the nonhuman primate brain, [^{11}C]Cimbi-36 was showed to be selective for 5-HT_2 receptors as ketanserin effectively blocked binding in all brain regions. Also, the cortical binding of [^{11}C]Cimbi-36 was found selective for 5-HT_{2A} receptors as binding in these regions was unaffected by selective 5-HT_{2C} receptor blockade.[15] This observation attested to the high relative density of 5-HT_{2A} receptors compared with 5-HT_{2C} in the cerebral cortex. Furthermore, pilot data from nonhuman primate brain show that [^{11}C]Cimbi-36 binding indeed is decreased after fenfluramine-induced increases in 5-HT levels,[16] suggesting that also at the 5-HT_{2A} receptor agonist radioligands are more sensitive to neurotransmitter release as compared with antagonist radioligands. We here present validation of [^{11}C]Cimbi-36 as the first successful 5-HT_{2A} receptor agonist PET radioligand in the human brain, and studies to determine the sensitivity of [^{11}C]Cimbi-36 to acute changes in 5-HT levels in the human brain are ongoing.

MATERIALS AND METHODS

Subjects

Twenty-nine healthy volunteers (mean age 23.0 ± 5.1 years, 15 males) were included in the study. Study participants were recruited through online and newspaper advertisements. Participants with prior or current psychiatric or neurologic diseases or severe traumatic brain injury were excluded from the study. None of the subjects took psychoactive medications, nor did they have prior or current substance or alcohol abuse as evaluated by interview. On the day of PET scanning, urine samples were screened for the presence of seven classes of abusive drugs (Rapid response Multi-Drug; BTNX Inc., Toronto, Ontario, Canada) and all subjects tested negative. The study was approved by the ethics committee for the Capital Region of Denmark (Journal no.: H-4-2012-105), and the first-in-human use of [^{11}C]Cimbi-36 was approved by the Danish Health and Medicines Authority (EudraCT number: 2012-002056-16). Arterial blood samples were obtained from a catheter placed in the radial artery, and arterial input measurements of parent compound, involving radiometabolite analyses using high-performance liquid chromatography (HPLC) were obtained in all participants. Blood samples acquired at the time of the PET scanning were tested with routine blood biochemistry and the outcomes were unremarkable. During PET scanning, subjects were monitored with 3-lead electrocardiography and pulse oximetry, and blood pressure was measured at regular intervals using a cuff around the upper arm.

Magnetic Resonance Imaging

All subjects were magnetic resonance imaging (MRI) scanned in a 3T Siemens Magnetom Verio scanner (Siemens AG, Erlangen, Germany) using a Siemens 32-channel head coil. Structural T1- and T2-weighted images (T1 protocol: Isotropic 0.9 × 0.9 × 0.9 mm resolution, repetition time = 1,900 ms, echo delay time = 2.32 ms, inversion time = 900 ms, and flip angle = 9°. T2 protocol: Isotropic 1 × 1 × 1 mm resolution, repetition time = 3,200 ms, echo delay time = 409 ms) were recorded for each subject, and based on these, a segmented magnetic resonance image was produced with vbm8 in SPM8 (Welcome Department of Imaging Neuroscience, London, http://www.fil.ion.ucl.ac.uk/spm) to mask gray matter in the subsequent automated extraction of tissue time-activity curves.

Radiochemistry

[^{11}C]Cimbi-36 was produced as previously described[11] with minor modifications (see Supplementary Figure 1). Briefly, [^{11}C]methyl triflate was transferred in a stream of helium to a 1.1-mL vial containing 0.1 to 0.2 mg of the labeling precursor (tert-butyl 4-bromo-2,5-dimethoxyphenethyl (2-hydroxybenzyl)carbamate, Cimbi-37) and 2 μL 2 mol/L NaOH in 300 μL acetone. The resulting mixture was heated at 40°C for 30 seconds to allow for complete reaction of the [^{11}C]methyl triflate followed by addition of 250 μL trifluoroacetic acid/acetone (1:1) and heating at 80°C for 5 minutes to hydrolyze the protecting group on the nitrogen. After neutralization with a mixture of 750 μL 2 mol/L NaOH and 3.7 mL 0.082% phosphoric acid, the reaction mixture was purified by HPLC (Waters Xterra C18, Waters Corp., Milford, MA, USA, 2.5 μm, 50 × 10 mm; eluent 25/75 ethanol/0.082% phosphoric acid; flow rate 9 mL/min, column temperature 60°C). Cimbi-36 reference compound and labeling precursor were synthesized as previously reported.[11,12]

The fraction corresponding to the radiolabeled product (retention time 3.7 minutes) was collected by allowing the HPLC eluent to flow directly through a 0.22-μm sterile filter (Millex GV; Millipore, Billerica, MA, USA) into a 20-mL glass vial containing 9 mL sterile phosphate-buffered saline solution (pH 7), giving a 14-mL sterile solution of [^{11}C]Cimbi-36 containing around 7% w/v ethanol. The total synthesis time after end of bombardment was ~30 minutes, yielding 1.0 to 3.5 GBq of [^{11}C]Cimbi-36 with radiochemical purity of >95% and specific radioactivity in the range of 240 to 1400 GBq/μmol at the end of synthesis. Quality control procedures were performed on each batch of [^{11}C]Cimbi-36 before release for human use and sterility and endotoxin tests were performed retrospectively.

Positron Emission Tomography Scanning

All study participants were scanned in a high-resolution research tomography PET scanner (CTI/Siemens, Knoxville, TN, USA) for 2 hours after a [^{11}C]Cimbi-36 bolus injection ($n = 29$; injected activity: 500 ± 117 MBq; injected cold Cimbi-36 dose: 0.83 ± 0.51 μg). The PET scanning began at the time of injection. No side effects that could be ascribed [^{11}C]Cimbi-36 injections were observed in the subjects. Five subjects received a per oral (p.o.) blocking dose of 10 or 20 mg ketanserin (Ketansin, Janssen-Cilag, The Netherlands) 48 ± 7 minutes before a second [^{11}C]Cimbi-36 PET scan with the same PET protocol. No adverse reactions that could be related to ketanserin administration were observed.

Positron emission tomography images were reconstructed using an iterative method as previously reported[17] (OP-OSEM3D with resolution modeling, 10 iterations, and 16 subsets) into 45 dynamic frames (6 × 10 seconds, 6 × 20 seconds, 6 × 60 seconds, 8 × 120 seconds, 19 × 300 seconds). Images consisted of 207 planes of 256 × 256 voxels of 1.22 × 1.22 × 1.22 mm^3. All PET images were motion corrected using the AIR (Automated Image Registration, v. 5.2.5, LONI, UCLA, http://bishopw.loni.ucla.edu/air5/) software where all frames were aligned to the first 5-minute frame, and no partial-volume correction was applied. Tissue time-activity curves were automatically extracted from a set of 45 distinct regions of interest (ROIs) using a data pipeline similar to previously reported.[18] Briefly, unfiltered PET images were coregistered and aligned to the subject's T1-weighted MRI image in SPM, and the segmented MRI images were also loaded before time-activity curves in gray matter were extracted for each ROI. Coregistration and ROI placement were visually inspected for each subject by overlaying ROIs on PET and MRI images. Larger and functionally determined ROIs were also defined as volume-weighted means: striatum as the mean of caudate nucleus and putamen; frontal cortex as the mean of orbitofrontal cortex, superior frontal gyrus, and medial inferior frontal gyrus; temporal cortex as the mean of superior temporal gyrus and medial inferior temporal gyrus; while neocortex includes all cerebral cortex ROIs. For the time-activity curves, standardized uptake values (SUVs) were obtained by normalizing radioactive concentrations in ROI (extracted as kBq/mL) to the injected dose per body weight (in kBq/g) yielding the unit g/mL.

During the first 10 minutes after injection, radioactivity in whole blood was continuously measured in 2-second intervals using an Allogg ABSS autosampler (Allogg Technology, Mariefred, Sweden) counting coincidences in a lead-shielded detector (flow: 8 mL/min). Also, blood samples were drawn manually 2.5, 5, 10, 15, 20, 30, 40, 50, 70, 90, 105, and 120 minutes after injection. Plasma was obtained by centrifugation (1,500 × *g* for 7 minutes at 4°C) of arterial whole blood. Radioactivity in whole blood and plasma was measured using a well counter (Cobra 5003; Packard Instruments, Meriden, CT, USA), which was cross-calibrated to the high-resolution research tomography scanner and to the autosampler. All samples were decay corrected to the time of radioligand injection. Radiolabeled parent compound and metabolites were measured in the discrete samples as described below.

Radiometabolite Measurements

The fraction of radioactivity corresponding to unchanged [^{11}C]Cimbi-36 and its radiometabolites was determined by direct injection of plasma in a column-switching radio-HPLC system as previously described.[19] Before analysis by radio-HPLC, the plasma samples were filtered through a syringe filter (Whatman GD/X 13 mm, PVDF membrane, 0.45 μm pore size; Frisenette ApS, Knebel, Denmark) and up to 4 mL of plasma was used directly. Eluent from the HPLC system was passed through the radiochemical detector (Posi-RAM Model 4; LabLogic, Sheffield, UK) for online detection of radioactive metabolites and parent tracer. The area under peaks corresponding to radiometabolites and parent compounds was quantified and expressed as a percentage of the sum of all detected areas using Chromeleon software version 6.80 (Thermo Fisher Scientific, Hvidovre, Denmark). To increase sensitivity in the later samples with low levels of radioactivity (40- to 120-minute samples), eluents (10 mL) from the HPLC were collected with a fraction collector (Foxy Jr FC144; Teledyne, Lincoln, NE, USA), and fractions were counted offline in a gamma well counter (2480 Wizard2 Automatic Gamma Counter, Wallac Oy, Turku, Finland).

The free fraction of [^{11}C]Cimbi-36 in human plasma (f_P) was estimated by equilibrium dialysis in each subject. Plasma spiked with [^{11}C]Cimbi-36 was loaded into one side of the dialysis chamber and dialyzed against an equal volume of phosphate-buffered saline (135 mmol/L NaCl, 3.0 mmol/L KCl, 1.2 mmol/L $CaCl_2$, 1.0 mmol/L $MgCl_2$, and 2.0 mmol/L KH_2PO_4, pH 7.4) through a cellulose membrane (molecular weight cutoff: 10,000 Da) at 37°C. f_P was calculated as the ratio of radioactivity in the plasma and buffer phase after equilibrium between the chambers was reached (after 120 minutes).

Quantification of [^{11}C]Cimbi-36 Binding

Kinetic modeling was performed in PMOD version 3.0 (PMOD Technologies Ltd, Zürich, Switzerland) using radioactive concentrations in whole blood, plasma, and parent compound fraction as an input to fit tissue time-activity curves. All blood measurements were referenced to the time of injection. For the initial 10 minutes of scanning, arterial plasma radioactivities were calculated from whole blood measurements (from the Allogg autosampler) by correction with a linear function describing time development of the plasma/whole blood ratios in the first five manual blood samples of each subject. The parameters of this linear function ($Y = a \times t + b$ with Y being plasma/whole blood ratios and t being time in seconds) were on average: $a = 0.00018 \pm 0.00008$, $b = 1.16 \pm 0.08$; mean ± s.d., $n = 29$. All blood and plasma radioactivities were scaled to measurements obtained with the Cobra counter. Parent compound fraction was fitted well with a two-exponential function and that was subsequently used to correct plasma concentration to obtain the parent compound arterial input function at individual subject level in all participants. [^{11}C]Cimbi-36 distribution volumes (V_T) were derived from the one- and two-tissue compartment models (1TCM and 2TCM) fitting three (K_1, k_2, V_B) or five parameters (K_1, k_2, k_3, k_4, V_B), respectively, and delay of blood curves was optimized simultaneously with a average delay of 7.5 ± 3.3 seconds. [^{11}C]Cimbi-36 V_Ts were also calculated from linearization with Logan plot graphical analyses (GA). From V_T in target areas, the nondisplaceable binding potentials (BP_{ND}s) were calculated as $(V_T^{target} - V_T^{cerebellum})/V_T^{cerebellum}$. Also, BP_{ND}s were calculated with Logan plot noninvasive GA (NIGA),[20] multi-linear reference tissue model, and the simplified reference tissue model (SRTM)[21] using cerebellum as a reference tissue. Additionally, SRTM2 modeling[22] was performed using a fixed k_2' estimated using SRTM in neocortex. Goodness-of-fit was evaluated using the Akaike Information Criterion (AIC), and regions with >10% covariance of the final outcome measure were excluded from further analysis. For occupancy modeling, the effect of ketanserin pretreatment (difference between 2TCM V_T at baseline and drug administration, $V_T^{baseline} - V_T^{ketanserin}$) was plotted against 2TCM $V_T^{baseline}$ in the left and right hemisphere for the following regions: cerebellum, orbitofrontal cortex, superior frontal gyrus, occipital cortex, medial inferior frontal gyrus, anterior and posterior cingulate, thalamus, insula, caudate nucleus, putamen, amygdala, superior and medial inferior temporal gyrus, parietal cortex, sensory motor cortex, entorhinal cortex, and hippocampus. In the remaining analyses, volume-weighted averages of left and right hemispheres were used. The time stability of [^{11}C]Cimbi-36 kinetic modeling was investigated by truncating the tissue time-activity curves to simulate shorter scans. Subsequently, 2TC and SRTM modeling was repeated for shorter scan durations (100, 80, 60, and 40 minutes).

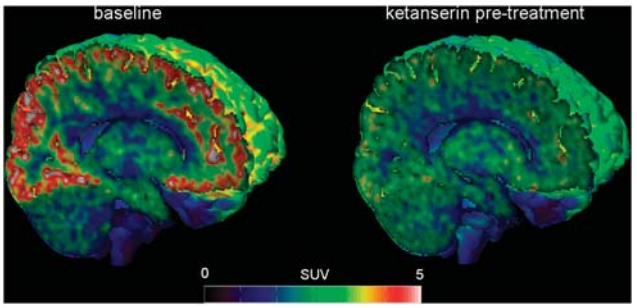

Figure 1. Representative [^{11}C]Cimbi-36 positron emission tomography (PET) brain images from a healthy volunteer at baseline and after ketanserin pretreatment. PET images show radioligand uptake from 40 to 120 minutes and scaled to standardized uptake values (SUVs; unit: g/mL), and images are superimposed on a magnetic resonance imaging (MRI) template of the brain.

RESULTS

[^{11}C]Cimbi-36 Distribution

[^{11}C]Cimbi-36 showed high uptake in the human brain and the radioligand distribution was in accordance with the expected cerebral 5-HT_{2A} receptor pattern in humans with high uptake in cortical regions and low uptake in cerebellum (Figure 1). The peak neocortical radioligand uptake was 3.8 ± 0.6 SUV (mean ± s.d., $n = 29$) (Figure 2). Time-activity curves showed that [^{11}C]Cimbi-36 concentrations in plasma had a rapid peak and washout, and although slower in brain tissue, peak and washout of [^{11}C]Cimbi-36 was also observed in all brain regions (Figure 2). In neocortex, the time after [^{11}C]Cimbi-36 injection to peak SUV was 49 ± 12 minutes (mean ± s.d., $n = 29$) meaning that in all subjects, reversible kinetics was present within the 120-minute scan time. Ten minutes after bolus injection with [^{11}C]Cimbi-36, an average of around 50% of the plasma radioactivity originated from the parent compound attesting to rapid metabolism of the radioligand (Figure 3), and after 120 minutes, ~10% intact tracer was left. Radiometabolites with shorter retention time than the parent compound were observed in human plasma after [^{11}C]Cimbi-36 injection (M2), and very polar metabolites (M1) were also observed (Figure 3B). Thirty minutes after radioligand injection, M2 metabolites constituted ~50% of the total radioactivity in human plasma.

Highest [^{11}C]Cimbi-36 binding in the human brain was found in the temporal cortices, this was the case regardless of the employed kinetic model (Table 1). While all cortical areas showed high [^{11}C]Cimbi-36 binding, intermediate [^{11}C]Cimbi-36 binding was found in hippocampus. [^{11}C]Cimbi-36 binding in other subcortical regions, for example, thalamus and striatum, was low. As expected, the lowest V_T values were found in cerebellum gray matter.

Kinetic Modeling of [^{11}C]Cimbi-36 Binding

Visual inspection revealed that the 2TCM fitted [^{11}C]Cimbi-36 tissue time-activity curves consistently better as compared with the 1TCM (Figure 2), and the 2TCM also yielded lower AIC values (Supplementary Table 1) indicating better fits with this model. The 2TCM produced higher V_T values than 1TCM and GA (see Table 1 and Figures 4A and 4B) pointing out a negative bias in these two latter models for determination of [^{11}C]Cimbi-36 V_T as compared with the gold standard of the 2TCM.

In the five subjects who received oral pretreatment with ketanserin, a highly significant decrease in 2TCM V_T was found in all cortical regions while it was unchanged in cerebellum (Figure 5), suggesting that cerebellum is a valid reference region. Hence, BP_{ND}s were quantified using cerebellum as a reference

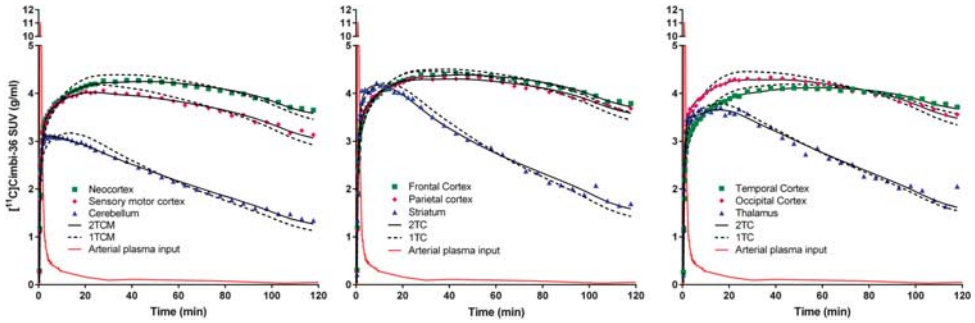

Figure 2. Representative [^{11}C]Cimbi-36 time-activity curves in plasma and brain tissue from a healthy volunteer. Radioactive concentrations in tissue and plasma are normalized to injected doses per kg bodyweight to attain standardized uptake values (SUVs). Brain tissue time-activity curves are fitted with one- and two-compartment models (1TCM and 2TCM).

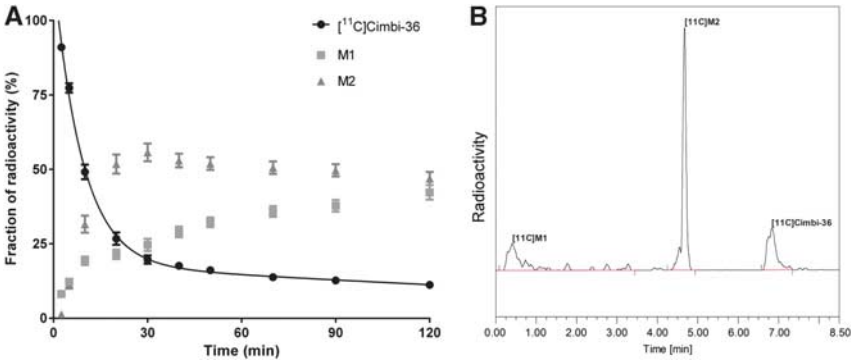

Figure 3. Radiometabolism of [^{11}C]Cimbi-36. (**A**) Time course of the percentage [^{11}C]Cimbi-36 parent compound fraction and radiometabolites measured in human arterial plasma. Points represent mean ± s.e.m. of 29 subjects, and the solid black indicates a two-exponential fit to the mean. (**B**) Representative radiochromatogram of human plasma sample taken 20 minutes after [^{11}C]Cimbi-36 injection.

tissue with SRTM, NIGA, and multi-linear reference tissue model (Figure 4). Additionally, the SRTM2 modeling resulted in very similar BP_{ND} values as compared with SRTM (linear regression between SRTM2 (Y) versus SRTM (X): $Y = 0.97 \times X + 0.046$, $r^2 = 0.99$). All the tested reference tissue models caused an underestimation of BP_{ND} of ~20% as compared with values quantified with 2TCM (Table 2). However, the BP_{ND}s measured with reference tissue models (NIGA and SRTM) and 2TCM were highly correlated between regions in individual subjects indicating that the negative bias of both models was predictable (Figure 4).

To investigate the necessity of a 120-minute scan time, we evaluated the [^{11}C]Cimbi-36 kinetic modeling after truncating tissue time-activity curves at different time points (100, 80, and 60 minutes). The neocortical V_T values derived from the 2TCM were stable with shorter scan durations, while lower V_T values were found in cerebellum as scan durations became shorter (Supplementary Figure 2). Thus, the neocortex BP_{ND} derived from 2TCM increased with decreasing time of PET data. For these shorter scan times, 2TCM was still superior as compared with 1TCM providing visually better fits and consistently lower AIC values. Conversely, the neocortex BP_{ND} derived from SRTM was decreased with decreasing scan duration, and this effect was already significant after decreasing PET scan time to 100 minutes (Supplementary Figure 2). Tissue time-activity curves shorter than 60 minutes generally did not produce reliable fits in any of the models applied as most regions displayed >10% covariance on the final outcome measure. The free [^{11}C]Cimbi-36 fraction (f_P) in human plasma was on average 2.9 ± 0.5% (mean ± s.d., $N = 28$).

Effect of Ketanserin on [^{11}C]Cimbi-36 Binding

Ketanserin caused a highly significant decrease in V_T across all cortical regions supporting 5-HT_{2A} receptor selectivity of [^{11}C]Cimbi-36 in these areas (Figure 5). No effect of ketanserin pretreatment was observed on [^{11}C]Cimbi-36 V_T in cerebellum supporting the use of this region as a reference region. To precisely quantify 5-HT_{2A} receptor occupancy by ketanserin, we made use of the occupancy plot in each subject receiving pretreatment before a second [^{11}C]Cimbi-36 PET scan. Plotting the effect of ketanserin on [^{11}C]Cimbi-36 brain uptake ($V_T^{baseline} - V_T^{ketanserin}$) against $V_T^{baseline}$ in individual brain regions produced highly significant correlations and positive regression slopes in all five subjects (Figure 6; Table 2). The 5-HT_{2A} receptor occupancy was here read as the slope of the occupancy plot of 2TCM V_T and it showed that ketanserin pretreatment led to an average receptor occupancy of 70 ± 10% (20 mg ketanserin, p.o., $n = 3$) and 62 ± 2% (10 mg ketanserin, p.o., $n = 2$). In the individual occupancy plots, the nondisplaceable distribution volume (V_{ND}) is read as the intercept with the x axis, and across five subjects we find stable V_{ND} values of 12.8 ± 1.4 mL/cm^3. Kinetic modeling of BP_{ND} at baseline and after ketanserin pretreatment derived from NIGA resulted in slightly lower measures of receptor occupancy (Table 2). The SRTM did not fit data from the blocked scans as these fits generally did not converge, thus receptor occupancy by ketanserin could not be quantified with this model. The ketanserin pretreatment also showed a pronounced effect on the [^{11}C]Cimbi-36 brain uptake and on the time course of the time-activity curves of [^{11}C]Cimbi-36; however, it did not affect the rate of [^{11}C]Cimbi-36 metabolism in plasma (data not shown).

Table 1. Total [^{11}C]Cimbi-36 V_T measures obtained by 1TCM and 2TCM and GA with arterial input function, and BP_{ND} obtained with 2TCM, NIGA, MRTM0 and SRTM

	Total distribution volumes (V_T)						*Nondisplaceable binding potential (BP_{ND})*							
	2TCM		*1TCM*		*GA*		*2TCM*		*NIGA*		*MRTM0*		*SRTM*	
	V_T (mL/cm^3)	*N*	V_T (mL/cm^3)	*N*	V_T (mL/cm^3)	*N*	BP_{ND} (unitless)	*N*	BP_{ND} (unitless)	*N*	BP_{ND} (unitless)	*N*	BP_{ND} (unitless)	*N*
Medial inferior temporal gyrus	40.3 ± 8.7	28	37.5 ± 8.1	29	36.2 ± 7.8	29	1.96 ± 0.23	28	1.54 ± 0.19	29	1.54 ± 0.16	18	1.51 ± 0.21	29
Orbito frontal cortex	40.2 ± 9.1	28	37.1 ± 8.4	29	35.4 ± 8.1	29	1.95 ± 0.24	28	1.52 ± 0.23	29	1.51 ± 0.23	8	1.63 ± 0.23	27
Temporal cortex	39.0 ± 8.4	29	36.8 ± 7.8	29	35.3 ± 7.3	29	1.88 ± 0.26	29	1.50 ± 0.19	29	1.50 ± 0.18	22	1.52 ± 0.21	29
Anterior cingulate	38.6 ± 8.1	28	36.8 ± 7.8	29	33.4 ± 7.7	28	1.88 ± 0.35	28	1.44 ± 0.28	29	1.22 ± 0.27	7	1.53 ± 0.28	26
Superior temporal gyrus	38.3 ± 8.0	29	36.0 ± 7.7	29	34.4 ± 7.1	29	1.84 ± 0.26	29	1.46 ± 0.20	29	1.46 ± 0.17	19	1.52 ± 0.22	29
Insula	37.1 ± 7.3	28	35.1 ± 6.9	29	32.5 ± 6.9	29	1.77 ± 0.26	28	1.39 ± 0.20	29	1.22 ± 0.18	4	1.51 ± 0.27	27
Medial inferior frontal gyrus	37.0 ± 7.4	29	35.1 ± 7.2	29	33.7 ± 6.5	27	1.74 ± 0.25	29	1.44 ± 0.20	29	1.46 ± 0.20	23	1.44 ± 0.22	29
Frontal cortex	36.9 ± 7.5	29	34.7 ± 7.0	29	33.4 ± 6.5	29	1.73 ± 0.24	29	1.41 ± 0.20	29	1.46 ± 0.19	25	1.43 ± 0.22	29
Superior frontal gyrus	36.1 ± 7.3	29	33.9 ± 6.9	29	32.4 ± 6.3	29	1.67 ± 0.26	29	1.35 ± 0.21	29	1.36 ± 0.22	20	1.37 ± 0.23	29
Neocortex	35.3 ± 7.1	29	33.6 ± 6.6	29	32.2 ± 6.2	29	1.62 ± 0.22	29	1.33 ± 0.17	29	1.39 ± 0.17	26	1.34 ± 0.19	29
Posterior cingulate	35.2 ± 7.9	29	34.0 ± 7.2	29	30.3 ± 7.0	29	1.60 ± 0.26	29	1.27 ± 0.23	29	1.09 ± 0.23	11	1.35 ± 0.17	27
Parietal cortex	34.5 ± 6.5	29	32.7 ± 6.3	29	31.5 ± 5.7	28	1.56 ± 0.24	29	1.29 ± 0.18	29	1.31 ± 0.21	23	1.29 ± 0.20	29
Occipital cortex	34.2 ± 7.0	29	33.1 ± 6.8	29	30.9 ± 6.2	29	1.53 ± 0.18	29	1.29 ± 0.15	29	1.26 ± 0.17	27	1.27 ± 0.17	29
Sensory motor cortex	28.6 ± 5.3	29	27.5 ± 5.1	29	26.2 ± 4.8	29	1.12 ± 0.20	29	0.97 ± 0.16	29	0.98 ± 0.18	18	0.95 ± 0.17	29
Entorhinal cortex	22.8 ± 5.1	27	21.5 ± 4.6	28	14.5 ± 5.0	15	0.67 ± 0.19	27	0.22 ± 0.22	29	dnf		dnf	
Hippocampus	21.9 ± 5.1	26	20.8 ± 4.6	29	18.4 ± 5.3	29	0.63 ± 0.21	26	0.44 ± 0.17	29	dnf		0.52 ± 0.12	6
Thalamus	18.7 ± 3.9	28	18.5 ± 3.9	29	17.1 ± 3.5	29	0.38 ± 0.10	28	0.34 ± 0.08	29	0.32 ± 0.06	25	0.33 ± 0.07	26
Striatum	17.2 ± 3.4	24	16.7 ± 3.2	29	15.2 ± 3.0	29	0.27 ± 0.10	24	0.25 ± 0.08	29	0.24 ± 0.06	27	0.25 ± 0.06	26
Cerebellum	13.6 ± 2.8	29	13.2 ± 2.7	29	11.5 ± 2.3	29								

1TCM, one-tissue compartment model; 2TCM, two-tissue compartment model; BP_{ND}, nondisplaceable binding potential; dnf, model did not fit in any of the subjects; GA, graphical analyses; MRTM0, multi-linear reference tissue model; NIGA, non-invasive GA; SRTM, simplified reference tissue model. Mean and s.d. of 29 subjects are shown for each model. All BP_{ND} measured uses cerebellum as reference tissue. *N* indicates the number of successful fits out of the 29 subjects with the indicated model in the given region.

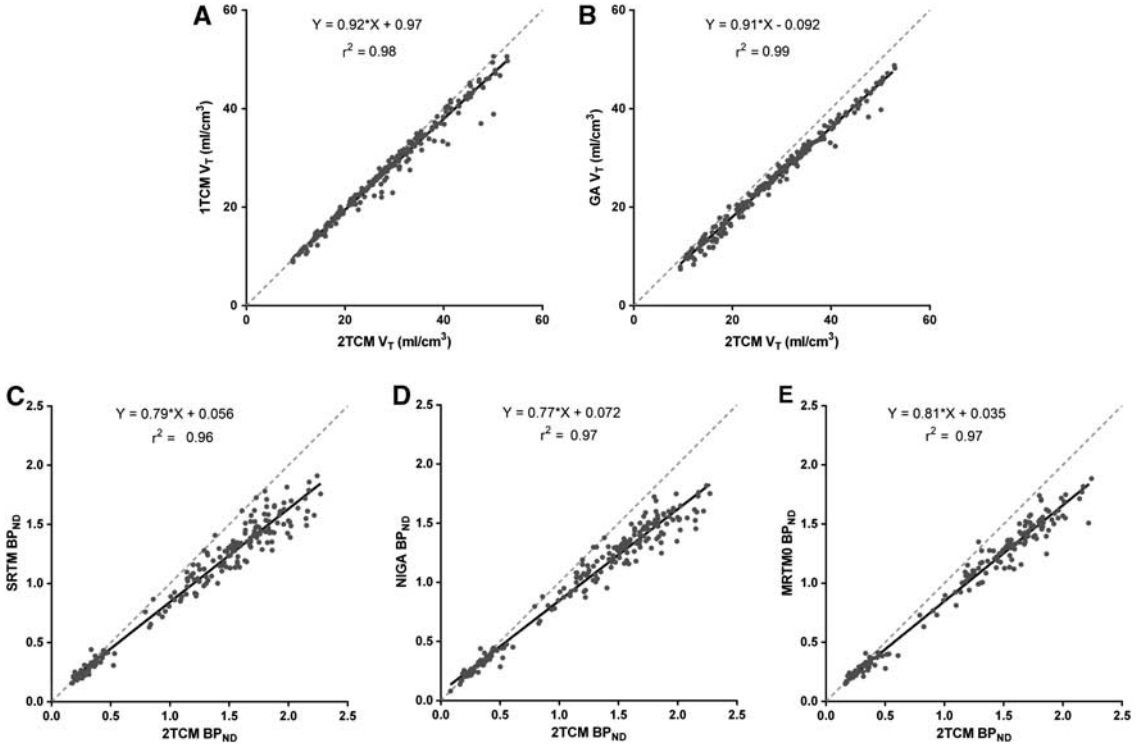

Figure 4. Correlations between outcome measures V_T (**A**, **B**) and nondisplaceable binding potential (BP_{ND}) (**C**, **D**) quantified with linear (**B**, **D**) and nonlinear (**A**, **C,** and **E**) models. Reference outcome measure was obtained with the two-tissue compartment model (2TCM) fitting five parameters (K_1, k_2, k_3, k_4, V_b). In V_T estimations, eight regions are analyzed from each of the 29 subjects: striatum, thalamus, frontal cortex, parietal cortex, somatosensory cortex, occipital cortex, temporal cortex, and cerebellum. Cerebellum was used as a reference region in BP_{ND} estimations, and with 2TCM, BP_{ND} was calculated as $(V_T^{target} - V_T^{cerebellum})/V_T^{cerebellum}$. Solid black lines show linear regressions and the regression equations are displayed in each plot. Dotted gray lines represent the line of identity. GA, graphical analyses; MRTM0, multi-linear reference tissue model; NIGA, noninvasive GA; SRTM, simplified reference tissue model.

DISCUSSION

We present the first successful agonist radioligand for PET imaging and quantification of 5-HT_{2A} receptors in the human brain. Measurement of 5-HT_{2A} receptor levels with [^{11}C]Cimbi-36 may be a more functionally relevant measure according to the hypothesis that agonists bind to the high affinity and active state of receptors selectively. We also expect that this 5-HT_{2A} receptor agonist may be sensitive to acute changes in 5-HT levels and thus cerebral [^{11}C]Cimbi-36 binding will be inversely correlated with endogenous neurotransmitter levels. Future studies will assess whether [^{11}C]Cimbi-36 has the potential to measure acute 5-HT release in the human brain.

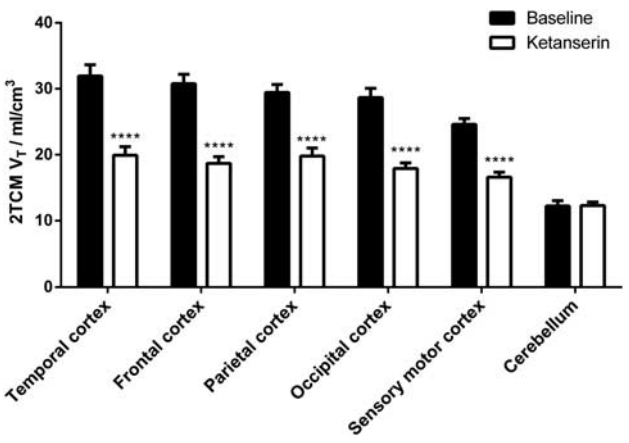

Figure 5. [^{11}C]Cimbi-36 V_T derived from the two-tissue compartment model (2TCM) at baseline ($n = 5$) and after per oral ketanserin pretreatment (10 mg, $n = 2$ or 20 mg, $n = 3$). ****$P < 0.0001$ refers to comparison of V_T in a two-way ANOVA with Bonferroni-corrected multiple comparisons test.

We found the 2TCM based on arterial input measurements optimal for quantification of [^{11}C]Cimbi-36 PET data from the human brain. The 2TCM fitted the tissue time-activity curves well, produced low AIC values, and V_T outcome values were very stable even when scan time was decreased. This is in line with previous data in nonhuman primates also finding that the 2TCM is the best for modeling [^{11}C]Cimbi-36 time-activity curves.[15] Practical challenges in a clinical setting related to the 2TCM-derived outcome measures are the long scanning time of 120 minutes and establishment of an arterial line. Through the ketanserin blocking study, we validated cerebellum as an appropriate reference tissue in humans indicating that the use of a reference tissue models would be possible for quantification of [^{11}C]Cimbi-36 thus omitting the need for arterial cannulation. That cerebellum is a valid reference tissue for quantification of 5-HT_{2A} receptor binding is in line with data from other antagonist PET radioligands.[23,24] However, we also found that BP_{ND} estimation with reference tissue modeling induces a negative bias as BP_{ND} quantified with NIGA and SRTM was ~20% lower as compared with BP_{ND} derived

Table 2. Summary of receptor occupancies measured with [^{11}C]Cimbi-36

Subject #	*Ketanserin dose (mg)*	*Ketanserin dose (mg/kg)*	*Occupancy plotting of 2TCM V_T*			*Reference tissue model (NIGA)*
			Receptor occupancy (%)	*V_{ND} (mL/cm^3)*	*R^2*	*Decrease in neocortex BP_{ND} after ketanserin (%)*[a]
1	20	0.27	81	12.6	0.95	60
2	20	0.25	64	12.7	0.91	64
3	20	0.20	65	11.7	0.90	64
4	10	0.15	60	11.9	0.85	54
5	10	0.12	63	15.3	0.93	59

2TCM, two-tissue compartment model; BP_{ND}, nondisplaceable binding potential; NIGA, noninvasive graphical analyses; V_{ND}, nondisplaceable distribution volume. [a]Calculated from neocortical binding potentials as $(BP_{ND}^{baseline} - BP_{ND}^{ketanserin})/BP_{ND}^{baseline}$.

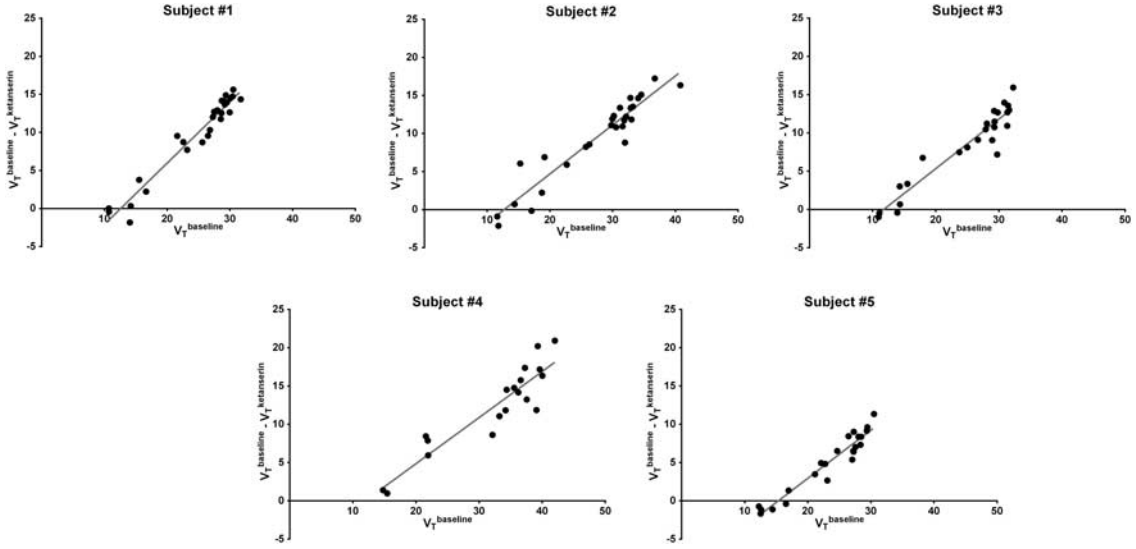

Figure 6. Individual occupancy plots of the effect of ketanserin on [^{11}C]Cimbi-36 binding in the human brain.

from the 2TCM. The negative bias in reference tissue models as compared with compartment models is a well-established observation with several other PET radioligands.[25,26] The SRTM assumes that tissue time-activity curves in the target as well as in the reference tissue can be described by the 1TCM,[21] and its underestimation of BP_{ND} has been suggested to originate in the violation of this assumption of 1TCM kinetics in the reference tissue.[27] That the negative bias of SRTM is caused by insufficiency in the 1TCM fitting of [^{11}C]Cimbi-36 PET data in cerebellum is in line with our finding that the 2TCM provided better fits and lower AIC values as compared with the 1TCM. The strong correlation between BP_{ND}s derived from 2TCM and the reference tissue models does however imply that the negative biases are predictable and that the percentage underestimation is fairly constant. Thus, in cross-sectional studies, for example, comparing 5-HT_{2A} receptor agonist binding with [^{11}C]Cimbi-36 between patients and controls, it should be sufficient to use a reference tissue model while collecting PET data for 120 minutes. This may aid clinical studies in patients where arterial cannulation is impractical. However, shortening scan time further increases the negative bias in the SRTM BP_{ND} estimation as well as it deteriorates the correlation with 2TCM BP_{ND}. Therefore, concurrent omission of the arterial line and shortened scan time is not recommended. Typical advantages of reference tissue approaches for receptor quantification also include higher test–retest reproducibility and lower interindividual variability. In the present analysis, we do indeed find a larger variation in V_T as compared with SRTM BP_{ND} in neocortex, but similar interindividual variability when comparing BP_{ND} derived from SRTM and 2TCM. Taken together, these results attests to the stable quantification of the arterial input function and compartmental modeling in healthy volunteers. However, further studies are warranted to address the test–retest reproducibility of quantification of [^{11}C]Cimbi-36 binding with compartment models versus reference tissue models.

We also tested the necessity for 120 minutes scan time by shortening time-activity curves and repeating kinetic modeling with 2TCM and SRTM after shortening scan data in intervals of 20 minutes. Where cortical 2TCM V_T outcome measures were stable with decreasing scan time, 2TCM BP_{ND} and particularly SRTM BP_{ND} measures were biased by decreasing the amount of data for kinetic modeling. The large negative bias found in SRTM BP_{ND} measures (which further increased with decreasing scan time) is likely explained by an increasing underestimation by the 1TCM in the target tissue when shortening tissue time-activity curves. Conversely, the positive bias in 2TC BP_{ND} measures with decreasing scan time is derived from insufficiency in the 2TCM to fit the time-activity curves in the reference region when these are shortened. Furthermore, SRTM quantification was compromised when measuring BP_{ND} in the ketanserin pretreated [^{11}C]Cimbi-36 scans as fits did not converge and failed to provide meaningful outcome measures. Conversely, the NIGA did provide reliable BP_{ND} measures in the blocked scans, and the estimates of receptor occupancies (quantified as $(BP_{ND}^{baseline} - BP_{ND}^{ketanserin})/BP_{ND}^{baseline}$) were coherent with values obtained with occupancy plotting of 2TCM V_Ts (Table 2). Previously, a small noise-induced positive bias in receptor occupancy measures from occupancy plotting has been shown,[28] which could be speculated to explain the marginally higher occupancies we found with occupancy plotting of 2TCM V_Ts as compared with the reference tissue model approach. Nevertheless, studies aiming to measure receptor occupancy after pharmacological interventions would be better advised in obtaining arterial input measures to enable 2TCM modeling and subsequent occupancy plotting, as this concurrently validates the assumption of regionally uniform occupancies. Furthermore, the occupancy plotting enables easy identification of regional outliers in receptor occupancy potentially caused by regional differences in receptor neurobiology or radioligand kinetics. In general, the choice of PET protocol and method for quantification in future clinical [^{11}C]Cimbi-36 studies may thus be impacted by study design: pharmacological intervention (particularly blocking) studies require arterial blood sampling and compartmental modeling whereas, for cross-sectional and longitudinal studies, using standard reference tissue models may suffice.

We found that ketanserin pretreatment effectively blocked a large fraction of the [^{11}C]Cimbi-36 binding across all cortical regions whereas we saw no effect in cerebellum. In the corresponding occupancy plots,[28] we found a significant linear relationship, indicating homogenous receptor occupancy across brain regions and validating the occupancy plot analysis to measure receptor occupancy with [^{11}C]Cimbi-36. Moreover, we found that the derived values of V_{ND} were not significantly different from the V_T in cerebellum, again confirming that this region is an appropriate reference tissue. With [^{11}C]Cimbi-36 PET in five subjects, we found that pretreatment with 10 or 20 mg ketanserin (p.o.) led to an average receptor occupancy of 67%. Pretreatment with 20 mg ketanserin lead to higher receptor occupancies than with 10 mg; however, more subjects and doses are necessary to fully elucidate the dose–occupancy relationship for ketanserin treatment, which was not the scope of this study. Previously, ketanserin pretreatment has been administered to humans in a couple of PET studies with [^{18}F]altanserin. Both after a ketanserin pretreatment p.o.[29] and a ketanserin challenge intravenously,[24] near-complete blocking effects were observed. Since these studies used higher doses of ketanserin (90 mg p.o. and 10 mg intravenously, respectively), the reported blocking effects are still regarded as coherent with the receptor occupancies found in the present study measured with [^{11}C]Cimbi-36. Also, the structural similarity between the blocking agent (ketanserin) and the radioligand (altanserin) may also contribute to the larger blocking effect found in previous studies. Chronic treatment with the atypical antipsychotic, quetiapine, in different clinically relevant doses resulted in average 5-HT_{2A} receptor occupancies of 64% measured with [^{18}F]altanserin PET, and no occupancies higher than 80% were measured,[30] emphasizing that the 5-HT_{2A} receptor occupancies measured in the current study are relevant in relation to 5-HT_{2A} receptor blockade.

The [^{11}C]Cimbi-36 V_T values in both target and reference regions of the human brain are relatively high and again higher when compared with values found in nonhuman primates.[15] In the occupancy plotting of [^{11}C]Cimbi-36 we found V_{ND} values around 12 mL/cm^3. With corresponding neocortical V_T values of 30 mL/cm^3 we thus found an approximate signal-to-noise ratio of 1.5 for quantifying 5-HT_{2A} receptor binding in cortical areas of the human brain with [^{11}C]Cimbi-36. This signal-to-background is at similar levels as the previous clinically validated PET radioligands such as [^{18}F]altanserin,[24] although the ratio is lower for [^{11}C]Cimbi-36 than that for [^{11}C]MDL100907,[23,25] as has also been reported in the direct comparison between the radioligands in the nonhuman primate brain.[15]

[^{11}C]Cimbi-36 has similar affinities for 5-HT_{2A} and 5-HT_{2C} receptors,[11] and in nonhuman primates it was showed that this radioligand could selectively image 5-HT_{2C} receptors in the choroid plexus and 5-HT_{2A} receptors in the cerebral cortex.[15] Further investigation of [^{11}C]Cimbi-36 binding in humans is necessary to tease out its 5-HT_{2C} receptor component, possibly by selective 5-HT_{2C} receptor blockade or by direct comparison with a PET radioligand with higher selectivity for 5-HT_{2A} over 5-HT_{2C} receptors.

After intravenous injection, [^{11}C]Cimbi-36 metabolized rapidly, and the rate of metabolism is similar between pigs,[11] monkeys,[15] and humans (present study) as quantified by a time-dependent decrease in the parent fractions. However, the route of metabolism may differ between species: we did find a more pronounced accumulation of radiolabeled metabolites with the highest

retention time (M2) in human plasma as compared with in pigs and monkeys. Further studies are needed to resolve the identity of these metabolites, and if species differences in their formation are present. However, we have previously shown that [^{11}C]M2 radiometabolites have very little if any accumulation in homogenized pig brain tissue as compared with pig plasma obtained at the same time after radioligand injection.[11] When scan duration was reduced from 120 minutes to 60 minutes, V_{ND} as measured by 2TCM V_T in cerebellum was decreased by ~3% (Supplementary Figure 2), and we cannot completely rule out that this may be due to lipophilic metabolites entering the brain at late time frames. However, this effect may also be due to a bias in the 2TCM at shorter scan times, and in any case it is a minor contribution to V_{ND}. Generally, many of the *in vivo* properties found with [^{11}C]Cimbi-36 in humans, for example, f_P and V_B, were concordant with results obtained in monkeys,[15] although the peak cortical uptake in humans was higher as compared with monkeys (3.8 SUV versus 1.7 to 2.6 SUV) with this peak cortical uptake being attained more slowly (~50 minutes versus ~20 minutes). Very similar cortical BP_{ND} values (referenced to cerebellum) were also found with [^{11}C]Cimbi-36 in humans and monkeys,[15] and these values are higher than what was previously observed in the pig brain.[11] This can be attributed to a relatively high concentration of 5-HT_{2A} receptors in the pig cerebellum which was also recently described.[31]

In summary, we have shown that the novel receptor agonist PET radioligand, [^{11}C]Cimbi-36, successfully labeled 5-HT_{2A} receptors in the human brain. We show kinetic models suitable for quantification of [^{11}C]Cimbi-36 binding, and we show that ketanserin pretreatment blocks [^{11}C]Cimbi-36 binding in the cerebral cortex, with no effects in cerebellum. When used cautiously, and with the notion of the observed negative biases, reference tissue model such as SRTM and NIGA may be used for [^{11}C]Cimbi-36 quantification in a clinical setting. This novel method enables studies on 5-HT_{2A} receptor agonist binding in larger populations or patient samples, including investigations of the sensitivity of cerebral [^{11}C]Cimbi-36 binding to changes in endogenous levels of 5-HT in the human brain.

DISCLOSURE/CONFLICT OF INTEREST

The authors declare no conflict of interest.

ACKNOWLEDGMENTS

The excellent technical assistance of Lone Ibsgaard Fryer, Bente Dall, Gerda Thomsen, Martin Korsbak Madsen, Svitlana Olsen, and Mikkel Lohmann Schiøtt is gratefully acknowledged.

REFERENCES

1 Gonzalez-Maeso J, Sealfon SC. Psychedelics and schizophrenia. *Trends Neurosci* 2009; **32**: 225–232.
2 Bhagwagar Z, Hinz R, Taylor M, Fancy S, Cowen P, Grasby P. Increased 5-HT(2A) receptor binding in euthymic, medication-free patients recovered from depression: a positron emission study with [(11)C]MDL 100,907. *Am J Psychiatry* 2006; **163**: 1580–1587.
3 Frokjaer VG, Mortensen EL, Nielsen FA, Haugbol S, Pinborg LH, Adams KH *et al.* Frontolimbic serotonin 2A receptor binding in healthy subjects is associated with personality risk factors for affective disorder. *Biol Psychiatry* 2008; **63**: 569–576.
4 Paterson LM, Tyacke RJ, Nutt DJ, Knudsen GM. Measuring endogenous 5-HT release by emission tomography: promises and pitfalls. *J Cereb Blood Flow Metab* 2010; **30**: 1682–1706.
5 Skinbjerg M, Sibley DR, Javitch JA, bi-Dargham A. Imaging the high-affinity state of the dopamine D2 receptor in vivo: fact or fiction? *Biochem Pharmacol* 2012; **83**: 193–198.
6 Paterson LM, Kornum BR, Nutt DJ, Pike VW, Knudsen GM. 5-HT radioligands for human brain imaging with PET and SPECT. *Med Res Rev* 2013; **33**: 54–111.
7 Narendran R, Mason NS, Laymon CM, Lopresti BJ, Velasquez ND, May MA *et al.* A comparative evaluation of the dopamine D(2/3) agonist radiotracer [11C](-)-N-propyl-norapomorphine and antagonist [11C]raclopride to measure amphetamine-induced dopamine release in the human striatum. *J Pharmacol Exp Ther* 2010; **333**: 533–539.
8 Hirani E, Sharp T, Sprakes M, Grasby P, Hume S. Fenfluramine evokes 5-HT2A receptor-mediated responses but does not displace [11C]MDL 100907: small animal PET and gene expression studies. *Synapse* 2003; **50**: 251–260.
9 Pinborg LH, Adams KH, Yndgaard S, Hasselbalch SG, Holm S, Kristiansen H *et al.* [18F]altanserin binding to human 5HT2A receptors is unaltered after citalopram and pindolol challenge. *J Cereb Blood Flow Metab* 2004; **24**: 1037–1045.
10 Quednow BB, Treyer V, Hasler F, Dorig N, Wyss MT, Burger C *et al.* Assessment of serotonin release capacity in the human brain using dexfenfluramine challenge and [18F]altanserin positron emission tomography. *Neuroimage* 2012; **59**: 3922–3932.
11 Ettrup A, Hansen M, Santini MA, Paine J, Gillings N, Palner M *et al.* Radiosynthesis and in vivo evaluation of a series of substituted (11)C-phenethylamines as 5-HT (2A) agonist PET tracers. *Eur J Nucl Med Mol Imaging* 2011; **38**: 681–693.
12 Ettrup A, Holm S, Hansen M, Wasim M, Santini MA, Palner M *et al.* Preclinical safety assessment of the 5-HT2A receptor agonist PET radioligand [11C]Cimbi-36. *Mol Imaging Biol* 2013; **15**: 376–383.
13 Poklis JL, Nanco CR, Troendle MM, Wolf CE, Poklis A. Determination of 4-bromo-2,5-dimethoxy-N-[(2-methoxyphenyl)methyl]-benzeneethanamine (25B-NBOMe) in serum and urine by high performance liquid chromatography with tandem mass spectrometry in a case of severe intoxication. *Drug Test Anal* advance online publication, 2 September 2013; doi:10.1002/dta.1522 (e-pub ahead of print).
14 Drug Enforcement Administration. Schedules of controlled substances: temporary placement of three synthetic phenethylamines into Schedule I. Final order. *Fed Regist* 2013; **78**: 68716–68719.
15 Finnema SJ, Stepanov V, Ettrup A, Nakao R, Amini N, Svedberg M *et al.* Characterization of [(11)C]Cimbi-36 as an agonist PET radioligand for the 5-HT2A and 5-HT2C receptors in the nonhuman primate brain. *Neuroimage* 2014; **84**: 342–353.
16 Finnema S, Ettrup A, Stepanov V, Nakao R, Yamamoto S, Varrone A *et al.* Pilot study on receptor binding and serotonin sensitivity of [11C]CIMBI-36 in monkey brain [abstract]. *J Nucl Med* 2011; **52**(Suppl 1): 495.
17 Sureau FC, Reader AJ, Comtat C, Leroy C, Ribeiro MJ, Buvat I *et al.* Impact of image-space resolution modeling for studies with the high-resolution research tomograph. *J Nucl Med* 2008; **49**: 1000–1008.
18 Svarer C, Madsen K, Hasselbalch SG, Pinborg LH, Haugbol S, Frokjaer VG *et al.* MR-based automatic delineation of volumes of interest in human brain PET images using probability maps. *Neuroimage* 2005; **24**: 969–979.
19 Gillings N. A restricted access material for rapid analysis of [11C]-labeled radiopharmaceuticals and their metabolites in plasma. *Nucl Med Biol* 2009; **36**: 961–965.
20 Logan J, Fowler JS, Volkow ND, Wang GJ, Ding YS, Alexoff DL. Distribution volume ratios without blood sampling from graphical analysis of PET data. *J Cereb Blood Flow Metab* 1996; **16**: 834–840.
21 Lammertsma AA, Hume SP. Simplified reference tissue model for PET receptor studies. *Neuroimage* 1996; **4**: 153–158.
22 Wu Y, Carson RE. Noise reduction in the simplified reference tissue model for neuroreceptor functional imaging. *J Cereb Blood Flow Metab* 2002; **22**: 1440–1452.
23 Talbot PS, Slifstein M, Hwang DR, Huang Y, Scher E, bi-Dargham A *et al.* Extended characterisation of the serotonin 2A (5-HT2A) receptor-selective PET radiotracer 11C-MDL100907 in humans: quantitative analysis, test-retest reproducibility, and vulnerability to endogenous 5-HT tone. *Neuroimage* 2012; **59**: 271–285.
24 Pinborg LH, Adams KH, Svarer C, Holm S, Hasselbalch SG, Haugbol S *et al.* Quantification of 5-HT2A receptors in the human brain using [18F]altanserin-PET and the bolus/infusion approach. *J Cereb Blood Flow Metab* 2003; **23**: 985–996.
25 Meyer PT, Bhagwagar Z, Cowen PJ, Cunningham VJ, Grasby PM, Hinz R. Simplified quantification of 5-HT2A receptors in the human brain with [11C]MDL 100,907 PET and non-invasive kinetic analyses. *Neuroimage* 2010; **50**: 984–993.
26 Parsey RV, Slifstein M, Hwang DR, bi-Dargham A, Simpson N, Mawlawi O *et al.* Validation and reproducibility of measurement of 5-HT1A receptor parameters with [carbonyl-11C]WAY-100635 in humans: comparison of arterial and reference tisssue input functions. *J Cereb Blood Flow Metab* 2000; **20**: 1111–1133.
27 Slifstein M, Parsey RV, Laruelle M. Derivation of [(11)C]WAY-100635 binding parameters with reference tissue models: effect of violations of model assumptions. *Nucl Med Biol* 2000; **27**: 487–492.

28 Cunningham VJ, Rabiner EA, Slifstein M, Laruelle M, Gunn RN. Measuring drug occupancy in the absence of a reference region: the Lassen plot re-visited. *J Cereb Blood Flow Metab* 2010; **30**: 46–50.

29 Sadzot B, Lemaire C, Maquet P, Salmon E, Plenevaux A, Degueldre C *et al*. Serotonin 5HT2 receptor imaging in the human brain using positron emission tomography and a new radioligand, [18F]altanserin: results in young normal controls. *J Cereb Blood Flow Metab* 1995; **15**: 787–797.

30 Rasmussen H, Ebdrup BH, Erritzoe D, Aggernaes B, Oranje B, Kalbitzer J *et al*. Serotonin2A receptor blockade and clinical effect in first-episode schizophrenia patients treated with quetiapine. *Psychopharmacology (Berl)* 2011; **213**: 583–592.

31 Hansen HD, Ettrup A, Herth MM, Dyssegaard A, Ratner C, Gillings N *et al*. Direct comparison of [(18) F]MH.MZ and [(18) F] altanserin for 5-HT2A receptor imaging with PET. *Synapse* 2013; **67**: 328–337.

Supplementary Information accompanies the paper on the Journal of Cerebral Blood Flow & Metabolism website (http://www.nature.com/jcbfm)